IEEE Access
Multidisciplinary | Rapid Review | Open Access Journal

Received May 30, 2022, accepted June 7, 2022, date of publication June 13, 2022, date of current version June 17, 2022.

Digital Object Identifier 10.1109/ACCESS.2022.3182805

Uncertainty-Aware Energy Management Strategy for Hybrid Electric Vehicle Using Hybrid Deep Learning Method

TAO ZHANG, CHUNQING ZHAO, XIAOXIA SUN, MIN LIN, AND QIDI CHEN
China North Vehicle Research Institute, Beijing 100072, China
Corresponding author: Xiaoxia Sun (sun_xiaoxia1983@163.com)

This work was supported by the National Natural Science Foundation of China under Grant 52102445.

ABSTRACT Energy management strategy (EMS) is important to ensure energy-saving performance of hybrid electric vehicle (HEV). However, the power coupling property between different power sources, together with stochastic power demand fluctuation poses great challenges for EMS to achieve desirable performance in real-world scenario. This paper presents an uncertainty-aware energy management strategy for HEV. A speed predictor combining convolutional neural network and long short-term memory neural network is proposed to extract temporal features that could reveal speed change mechanism. Then an online self-adaptive transition probability matrix is constructed to estimate the speed prediction uncertainty. Tube model predictive control (tube-MPC) is finally used to solve the optimization control problem in a receding horizon manner. The robust set introduced in the tube-MPC greatly enhances the optimality and robust-ness of the control sequence under the scenario with speed prediction uncertainty. Simulations are conducted to verify the effectiveness of the proposed method. Results show that the speed prediction accuracy is 47.4% and 23.1% higher than exponential decay rate prediction model and autoregressive integrated moving average model respectively. Compared with traditional rule-based and MPC method, the proposed tube-MPC method could achieve 10.7% and 3.0% energy-saving performance improvement in average.

INDEX TERMS Uncertainty-aware energy management, hybrid electric vehicle, hybrid deep learning, tube model predictive control.

I. INTRODUCTION

Energy shortage is one of the main problems confronted by all countries around the world in the 21st century [1]. As the main roles in modern transportation, internal combustion engine vehicles are not only the main consumer of energy, but also one of the main sources of environmental pollutants [2]. For traditional internal combustion engines, the efficiency of diesel engines is generally lower than 55%, and that of gasoline engines is even no higher than 45% [3]. Therefore, in order to promote the energy-saving and low-carbon development of transportation, in recent years, the whole automobile industry is transforming from ''oil-dependent'' to ''new energy-dependent'', and hybrid electric vehicle (HEV) is the first step in the transformation of transportation electrification [4], [5].

The associate editor coordinating the review of this manuscript and approving it for publication was Vitor Monteiro.

The primary goal of HEV is to improve the efficiency of power system and reduce fuel consumption. When the powertrain configuration is given, the most important factor on HEV fuel consumption is the power allocation ratio between the engine and the electrical system. Energy management strategy (EMS) needs to coordinate the power distribution between the engine and the electrical system under the constraint that the power demand is satisfied. For the same vehicle model and the same driving cycle, the fuel consumption corresponding to different energy management strategies can vary by 20% [6]. Thus, it is of great significance to study the EMS of HEV.

Generally speaking, EMS can be divided into two categories: rule-based and optimization based. In terms of rule-based methods, Dextreit *et al.* [7] divided the engine working area into high load, medium load and medium and low load areas, and determined the working mode based on the calculated demand power according to the driver's accelerator

pedal opening and opening change rate. Li [8] proposed an instantaneous rule-based optimal energy allocation algorithm considering the impact of the timing of engine entering/exiting the powertrain on the fuel economy. The rule-based control method has the advantages of low computation and easy implementation, so it has been widely used in modern mass-produced HEV [9]–[11]. However, the rule-based method also has obvious disadvantage. The designed control strategy usually has the optimality only under the specific condition used for rule calibration, while the real situation the vehicle will undergo is very complex. The rule-based control algorithm lacks adaptability under non-standard working conditions and the energy-saving performance will be greatly weakened in real-world scenario [12].

Optimization-based algorithms are another kind of EMS that have been widely studied in recent years, including particle swarm optimization (PSO), genetic algorithm (GA), convex optimization and the most representative dynamic programming (DP) [13]–[16]. For example, Zhang *et al.* [17] used the optimization results of DP to improve the rule-based EMS and achieved better energy-saving effect. Correa *et al.* [18] used DP to find the optimal power distribution principle between engine and motor, and designed a fuzzy logic controller on the basis of considering SOC balance and driving style recognition. Although DP can obtain the global optimal solution, it needs to obtain future working conditions in advance and can only be realized in offline manner [19].

To further enhance the energy-saving performance, advanced researches incorporate speed prediction to make EMS has prior knowledge about future driving cycle, thus making optimal decision not only focus on current state but also consider future situations [20]–[22]. In addition, by substituting DP with reinforcement learning (RL) or model predictive control (MPC), control policy could be operated online [23], [24]. For example, Teng *et al.* [25] presented a predictive online energy management strategy for a parallel HEV based on velocity prediction and RL. Menglin *et al.* [26] adopts deep learning to predict future power demand, thus proposing an online adaptive EMS and realizing efficiency improvement. However, the future speed or power demand is affected by so many stochastic factors (including traffic flow, weather, driver's driving style) that the prediction uncertainty is unneglectable in real-world driving scenarios [27]–[29]. Although above methods could enhance energy-saving performance when prediction is accurate, their robustness under circumstance of uncertain prediction is still in question.

Several advanced EMS researches start to focus on uncertainty introduced by real-world stochastic factors. For example, Shangguan *et al.* [30] proposed a robust energy management for plug-in hybrid electric buses considering the uncertainties of driving cycles and vehicle mass using Pontryagin's minimum principle method. He *et al.* [31] incorporated the uncertainty of renewable energy and load when designing EMS for hybrid energy storage system. However, above methods do not work in a predictive manner.

To exploit the advantage of predictive EMS while considering the stochastic factors in real-world driving [32], [33], Zeng *et al.* [34] proposed a stochastic model predictive control-based EMS using the vehicle location, traveling direction, and terrain information of the area for HEVs running in hilly regions with light traffic. The stochastic property of road grade is modeled as a Markov chain. Zhao *et al.* [35] proposed a stochastic model predictive control (SMPC) method to exploit the potential performance of dual-motor coupling powertrain, where the uncertainty of velocity prediction is captured and modeled through a novel Signed Markov Chain Monte Carlo method. However, the optimization result output by traditional MPC or SMPC may deviate from the optimal control policy or fail to realize stable control if the uncertainty is not properly quantified. The robustness of proposed method may still confront with challenges when facing strong stochastic factors in dynamic traffic scenes.

Heavy reliance on a model makes traditional MPC or SMPC susceptible to modeling error and external disturbances, often leading to poor performance or instability. Robust MPC (RMPC) addresses this limitation (at the expense of additional computational complexity) by optimizing over control policies instead of open-loop control actions. Tube MPC is a tractable alternative that decomposes RMPC into an offline robust controller design and online open-loop MPC problem [36]. Fig.1 gives an intuitive illustration of tube-MPC. Given an ancillary control and associated robust control invariant tube Ω, a constraint-tightened version of the nominal MPC problem can be solved to generate an open-loop control input u^* and trajectory x^*. Even suspected to model uncertainty inference, the control sequence could constrain the system within tolerance scope Ω, ensuring the optimality and stability of the solution.

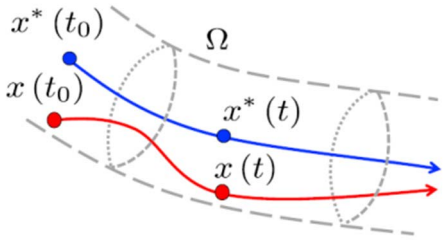

FIGURE 1. Illustration of tube-MPC. If the state x begins in Ω then it remains in Ω indefinitely for all realizations of the model error or external disturbance.

In addition, an uncertainty-aware speed predictor, which combines hybrid deep learning model with transition probability matrix (TPM) based estimation error quantification, is proposed to assist the application of tube-MPC. Thanks to the powerful automatic feature extraction ability of deep learning method, the proposed speed predictor could realize accurate speed prediction, which helps to enhance the stability and optimization of the result output by tube-MPC.

Generally, in this paper, a predictive uncertainty-aware EMS for HEV based on tube-MPC is proposed. Firstly, an adaptable online energy management framework is proposed for HEV, considering the uncertainties in speed prediction profiles. Secondly, a hybrid deep learning model is established to forecast the future information and the prediction errors are quantified via TPM. Thirdly, tube-MPC is adopted to optimize the control policy over a moving time window and the method's superiority is verified against some traditional EMS.

The remainder of this paper is organized as follows. Section II gives the general framework of the proposed uncertainty-aware EMS together with highlights of its innovation. Section III and section IV introduce two vital parts in the proposed EMS, namely hybrid deep learning-based speed prediction model and tube-MPC algorithm, respectively. The performance of the proposed method is well evaluated through simulation in Section V.

II. PREDICTIVE ONLINE ENERGY MANAGEMENT STRATEGY

Fig.2 shows the overall architecture of the predictive online energy management strategy. Firstly, at each step, history speed trajectory will be fed into the speed predictor to forecast the vehicle speed in a fixed-length future time window. Then, TPM will be combined with the speed prediction to give out the speed estimation error. Afterwards, tube-MPC is used to solve this tricky problem, which could ensure the stability of the control policy even under the uncertain speed prediction scenario. Finally, only the first of optimized control sequence $u(h)$ is executed on the system and system will transfer to a new state after control execution. The information of new state will be fed into the MPC controller for the control optimization at the next time step.

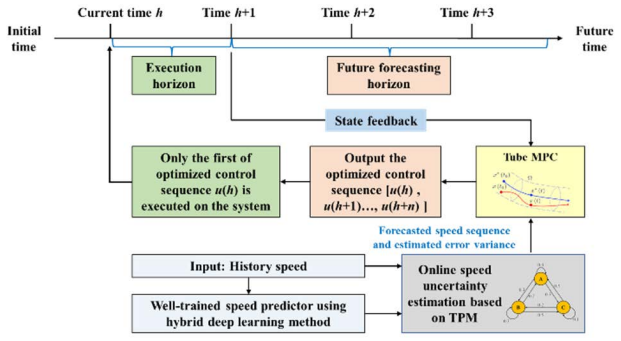

FIGURE 2. Architecture of the predictive online energy management strategy.

III. UNCERTAINTY-AWARE SPEED PREDICTION MODEL

Fig.3 gives the architecture of hybrid deep learning based speed prediction model. The input is first fed into the convolutional neural network (CNN) layer to extract high-dimensional features that can reflect the internal characteristics of speed change. Then max-pooling layer is used to down-sample the output to the patch that could highlight the most valuable features. Another set of CNN and max-pooling layer is added to further distill the features. Afterwards, long short term memory (LSTM) layer is appended to incorporate the extracted features for time series prediction. Finally, fully connected layer is adopted to realize final speed prediction. In order to compensate the speed prediction error, a TPM is accompanied with the hybrid network to realize awareness of uncertainty. Details of each part are described as follows.

A. INPUT LAYER

The general idea of the model is to use data from last several intervals to predict the speed in the future time window. Let m denotes the input data length, p denotes the number of input variables, then the input can be expressed as:

$$D_i = \begin{bmatrix} d_{var1}(h-m) & \cdots & d_{var1}(h) \\ \vdots & \ddots & \vdots \\ d_{varp}(h-m) & \cdots & d_{varp}(h) \end{bmatrix} \tag{1}$$

In this paper, the input variables include speed, acceleration, mean and standard deviation of speed over time window L ($L < m$), which means $p = 4$ here.

B. CNN AND MAX-POOLING LAYER

The calculation of CNN layer generally includes two steps [37]: first, convolution operation is carried out by multiplying convolution kernel with each small patch. Then nonlinear function is applied to realize de-linearization function. The values $z^l_{i,j,k}$ at the position (i, j) in the k-th characteristic diagram of the l-st layer are calculated as following equation:

$$z^l_{i,j,k} = w^l_k x^{l-1}_{i,j} + b^l_k \tag{2}$$

where w^l_k and b^l_k are the weight coefficient vector and offset of the k-th convolution kernel of the l-th layer respectively. The notations w and b used are also used in following equations to represent weight and offset vector when introducing LSTM layer. $x^{l-1}_{i,j}$ is a piece of input data centered on position (i, j) in layer $l-1$. The activation function is used to introduce nonlinearity into CNN, so that CNN can detect nonlinear characteristics. Let $a(\cdot)$ be a nonlinear activation function, then the activation values $a^l_{i,j,k}$ of the convolution features $z^l_{i,j,k}$ can be calculated according to following equation:

$$a^l_{i,j,k} = a(z^l_{i,j,k}) \tag{3}$$

Here, ReLU activation function is used.

The function of pooling layer is to summarize the features extracted from the convolution layer and compress the information, so that the feature range that CNN can extract could be much wider. Let the pooling function is denoted as $pool(\cdot)$, then for each characteristic graph $a^l_{i,j,k}$, we can get output $y^l_{i,j,k}$ as follows:

$$y^l_{i,j,k} = pool(a^l_{i,j,k}) \tag{4}$$

The kernel size of CNN and max-pooling layers are set as 2×2 in this paper.

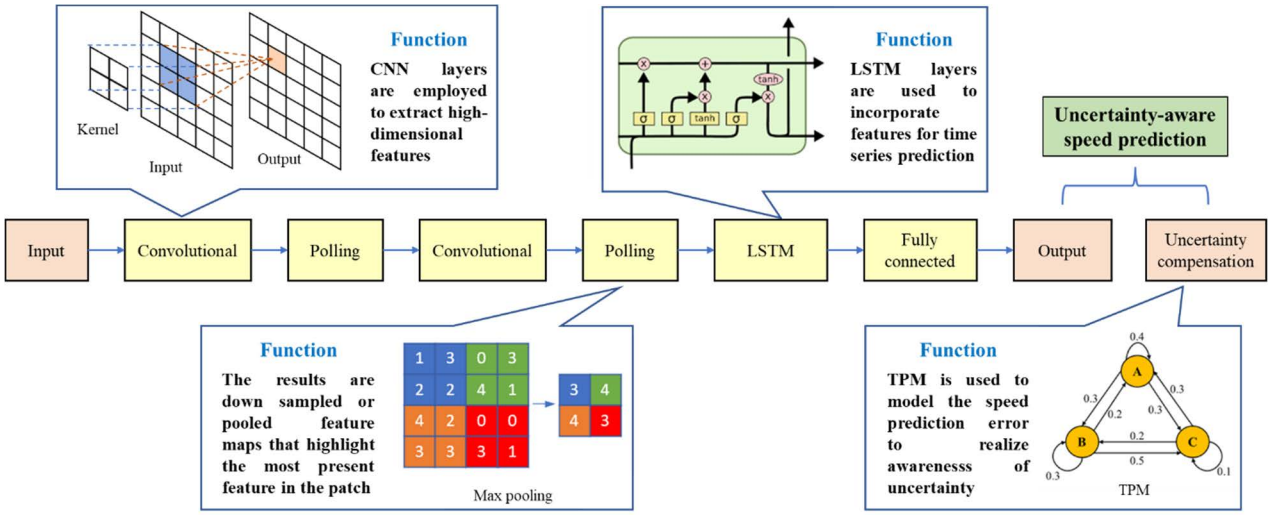

FIGURE 3. Architecture of the hybrid deep learning model.

C. LSTM LAYER

LSTM neural network is a special recurrent neural network (RNN), which is mainly to solve the problem of gradient disappearance in the process of long sequence training [38]. For each LSTM layer, it needs to process two states, namely hidden state a_m^i and memory state c_m^t. The candidate memory value $\tilde{c_m^t}$ of the m-th LSTM layer at a certain time t is:

$$\tilde{c_m^t} = \tanh(w_m^c \left[a_m^{t-1}, a_{m-1}^t\right] + b_m^c) \tag{5}$$

where a_m^{t-1} represents the activation value obtained from the same layer at the last time. a_{m-1}^t represents the activation value obtained from the last LSTM layer at the same time.

For the m-th LSTM layer, three gating operations, namely memory gate Γ_m^u, forget gate Γ_m^f and output gate Γ_m^o need to be recorded. These three gates determine the true memory value c_m^t and activation value a_m^t of the LSTM unit. Memory gate Γ_m^u and forget gate Γ_m^f of m-th LSTM layer can be obtained by following equations:

$$\Gamma_m^u = \sigma(w_m^u \left[a_m^{t-1}, a_{m-1}^t\right] + b_m^u) \tag{6}$$

$$\Gamma_m^f = \sigma(w_m^f \left[a_m^{t-1}, a_{m-1}^t\right] + b_m^f) \tag{7}$$

where σ represents sigmoid activation function. Then, the memory value c_m^t at time t of m-th layer can be obtained through two ways. One is generated by the candidate value at current time, the other is obtained from the memory value at previous time. They are controlled by the memory gate Γ_m^u, forget gate Γ_m^f as follows:

$$c_m^t = \Gamma_m^u \tilde{c_m^t} + \Gamma_m^f \tilde{c_m^{t-1}} \tag{8}$$

The hidden state a_m^t at time t of m-th layer can be obtained from the output gate Γ_m^o according to following equations:

$$\Gamma_m^o = \sigma(w_m^o \left[a_m^{t-1}, a_{m-1}^t\right] + b_m^o) \tag{9}$$

$$a_m^t = \Gamma_m^o c_m^t \tag{10}$$

The output sequence y^t is obtained from the last *softmax* activation layer:

$$y^t = softmax(a_M^t) \tag{11}$$

where M represents the total layers of LSTM.

D. OUTPUT LAYER WITH UNCERTAINTY COMPENSATION

The output of the hybrid deep learning model is the predicted speed over a future time window with length n, which means:

$$D_o = [v_p(h+1) \quad \cdots \quad v_p(h+n)] \tag{12}$$

In order to compensate the uncertainty inherent in speed prediction, online uncertainty-aware correction based on TPM is adopted here. Suppose the real speed at future time instance ζ is v^ζ, then:

$$v^\zeta = v_p^\zeta + v_e^\zeta \tag{13}$$

where v_p^ζ represents the predicted speed and v_e^ζ denotes the stochastic prediction error. Gaussian distribution is used to model the error property here, which means $v_e^\zeta \sim N(0, \sigma^2)$. Considering the assumption that speed change confirms to Markov property, then TPM can be used to model the speed transition process. An online TPM updating mechanism with forgetting factor φ is adopted here to track the uncertainty trend [39]:

$$P_{i,j}(L) = P_{i,j}(L-1) + \varphi[p_{i,j}(L) - P_{i,j}(L-1)] \tag{14}$$

where $P_{i,j}(L)$ represents the probability of the transition from v_i to v_j. $p_{i,j}(L) = 1$ if a transition from v_i to v_j occurs at time instant L, else equals to 0. The forgetting factor $\varphi \in (0, 1)$ is to determine the effective memory depth and control the rate of updating $P_{i,j}(L)$, which is set as 0.1 in this paper. After obtaining the TPM, speed chain can be sampled. In this paper, 10 chains with length 5 are sampled for each sampling instance, and the averaged standard deviation of the 10 chains is used to approximate the σ value.

The deep learning based hybrid model can be trained using Adam method offline and used for speed prediction online. The TPM can be updated online to track the time-varying and stochastic change of speed estimation error. it also needs to be mentioned here that more variables can be incorporated into the input and output layers if any other predictive information is needed for subsequent energy management application.

IV. TUBE-MPC BASED PREDICTIVE ONLINE ENERGY MANAGEMENT STRATEGY

To apply optimal control, HEV system model is prerequisite. Suppose HEV System with uncertainty can be described by following equation:

$$x\,(h+1) = f(x\,(h)\,,u\,(h)\,,w(h)) \tag{15}$$

where x denotes the state variables. u represents control variables. w is uncertain factor and refers to speed uncertainty in this paper. The detailed model of investigated HEV can be found in Appendix. In this paper, $x = [v_h, \text{SOC}, P_{veh}, v_{h+1}, v_{h+2}, \ldots v_{h+n}]$ and $u = [\text{mode}, T_{eng}, n_{eng}]$ (mode refers to electric drive mode, engine drive mode and hybrid mode).

In this paper, tube MPC with one-step look-ahead robust set is used to solve the above optimization problem online, which can achieve close optimal control performance even under the circumstance of stochastic interference. Generally, Tube MPC includes two parts, namely offline part and online part. The standard tube-based MPC algorithm is solved absolutely offline, and the only online calculations are to confirm which partition the current state lies in. In online part, different control laws will be selected according to different states so as to ensure that the state will be controlled within tolerant boundary under uncertainty scenario. Table.1 demonstrates the steps of the algorithm [40], [41].

TABLE 1. Tube MPC algorithm.

Algorithm: Tube MPC with one-step look-ahead robust set t

1) Offline part

Step 1: For the companion system without interference of Eq.(15), namely

$$x(h+1) = f(x(h), u(h))$$

Calculate the polyhedron invariant set sequence converging to the origin S_1, S_2, …, S_M and corresponding control coefficients K_1, K_2, …, K_M, set $S = \cup_{j=1}^{M} S_j$

Step 2: According to the feedback gain obtained in the previous step, calculate the sequence of the minimum robust control invariant set Z_1, Z_2, …, Z_M corresponding to each control gain, and select the minimum robust control invariant set as the interference invariant set Z_f in the tube sequence. The corresponding feedback control coefficient is K_f.

Step 3: Set $\bar{X} = X \ominus Z_f$ as the new state constraint ($\ominus$ denotes the Pontryagin difference of two sets), $\bar{U} = U \ominus K_f Z_f$ as the input constraint, calculate the control invariant set $\widetilde{\Omega_i}$ of the companion system corresponding to K_i. Thus, new terminal constraint set $\widetilde{\Omega} = \cup_{i=1}^{M} \widetilde{\Omega_i}$.

Step 4: Set $\widetilde{\Omega}$ as the new terminal constraint set and calculate the N-step look-ahead robust set $\tilde{E}_N^r(\Omega)$.

2) Online part

Step 1: Set the initial state $x(0) \in S$.

Step 2: for each time instance h, judge:

condition 1: if $x(h) \in Z_f$, set $x'(h) = 0, u'(h) = 0$ and control policy can be set as $u(h)=K_f x(h)$.

condition 2: if $x(h) \in \cup_{i=1}^{M} (\widetilde{\Omega_i}) \oplus Z_f, x(h) \notin Z_f$ ($\oplus$ denotes the Minkowski summation of two sets), then we can find $x(h) \in x'(h) \oplus Z_f$ and $x'(h) \in \cup_{i=1}^{M} \widetilde{\Omega_i}$ and set control as:

$$u(h) = K_i x'(h) + K_f\big(x(h) - x'(h)\big)$$

where $i \in \max\{j : x'(h) \in \widetilde{\Omega_j}\}, x'(h+1) = f(x'(h), u'(h))$.

condition 3: if $x(h) \in \tilde{E}_N^r(\Omega) \oplus Z_f, x(h) \notin \cup_{i=1}^{M} \widetilde{\Omega_i} \oplus Z_f$, set $x'(h) \in \tilde{E}_N^r(\Omega)$ and $x(h) \in x'(h) \oplus Z_f$, minimize the cost function to obtain the optimal control sequence $\min_{u'(h)} J(h)$ while subjecting to constraint:

$$\begin{cases} x'(h) \in \bar{X},\ u'(h) \in \bar{U} \\ f(x'(h),\ u'(h)) \in \begin{cases} \tilde{E}_N^r(\Omega) & i > 1 \\ \widetilde{\Omega} & i = 1 \end{cases} \\ x'(h+1) = f(x'(h),\ u'(h)) \\ x(h+1) = f(x(h), u(h), w(h)) \\ u(h) = u'(h) + K_f(x(h) - x'(h)) \end{cases}$$

where $i = \min\{j : x(h) \in \tilde{E}_N^r \oplus Z_f\}$. Iterate above process until i=1. Implement control policy switch according to $x(h) \in \tilde{E}_N^r(\Omega) \oplus Z_f$ and $x'(h) \in \cup_{i=1}^{M} \widetilde{\Omega_i}$.

Step 3: Measure the real and nominal system state at next time instance, set h=h+1 and return back to Step 2 until the system is stable.

V. VERIFICATION AND SIMULATION

In this section, effectiveness of the proposed method will be evaluated through simulation. Generally, two aspects of the method are discussed here. First, the accuracy of the proposed speed predictor using hybrid deep learning method will be compared with traditional methods including exponential decay rate prediction model and autoregressive integrated moving average model (ARIMA). Then the superiority of the proposed method will be highlighted compared with rule-based method and MPC method without considering the speed estimation uncertainty.

A. SPEED PREDICTION PERFORMANCE EVALUATION

In order to evaluate the accuracy of the proposed deep learning based speed prediction method, two conventional methods are used as benchmark here. The first method is exponential decay rate prediction model, which can be expressed by:

$$v_{h+i} = v_h \times (1+\varepsilon)^i \tag{16}$$

where v_h represents the starting speed at time point h. ε is the exponential decay factor and different ε values correspond to different vehicle speed decay rates. Here, ε is set as 0.002 through trial-and-error.

The second method is ARIMA (p, d, q), which is a commonly used linear forecasting approach, where p is the autoregressive form, q is the moving average window and d is the order of differencing. Here, d is assigned as 2, p and q are selected according to the auto-correlation and partial-correlation graph of the data.

Fig.4 compares the speed prediction accuracy of the three methods. The speed trajectory used for prediction is collected

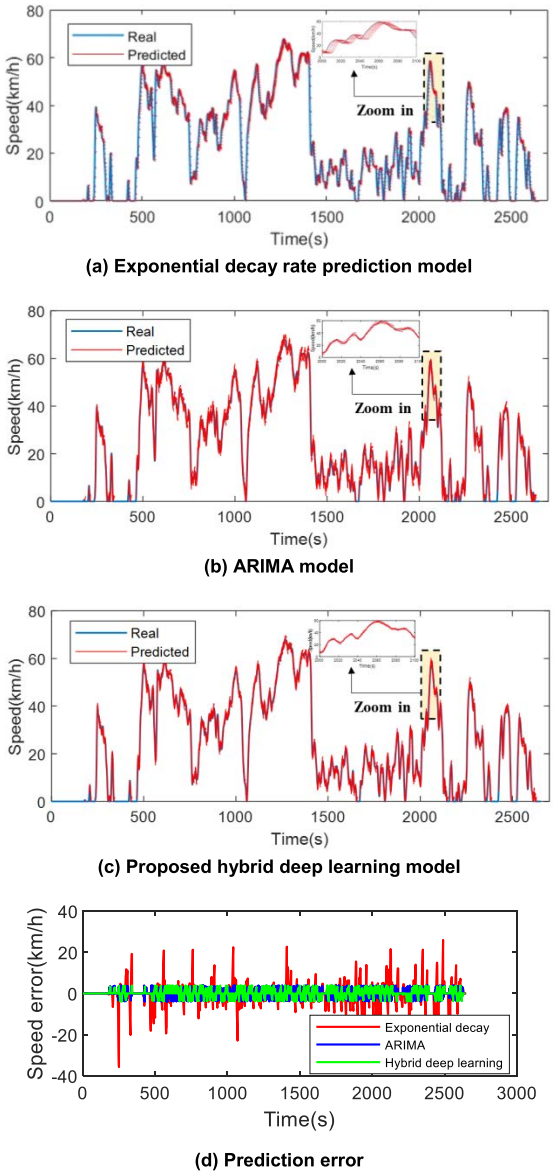

FIGURE 4. Speed prediction accuracy of three methods.

from a real-world driving in Beijing [42]. It can be seen from the figure that for exponential decay rate prediction model, the predicted speed shows an exponential attenuation trend in the future time window, but obvious differences exist between the real and predicted speed trajectories, especially when there is a sharp speed change around stop, which means this model is insufficient to capture the sophisticated dynamic change of speed variation. The average prediction error is 3.8km/h in this scenario. For the ARIMA model, through the fitting of moving window, the speed prediction deficiency of the above exponential decay rate prediction model can be solved to a certain extent and the prediction error is decreased to 2.6km/h. However, there is still room to improve the speed prediction accuracy. The final proposed hybrid deep learning method achieves highest prediction accuracy benefited from the powerful data mining and processing abilities of CNN and LSTM, which can extract and learn temporal features from historical data. The prediction error is only 2.0km/h in this scenario.

TABLE 2. Energy-saving performance of different algorithms.

Group	EMS	SOC init	SOC final	Neng	Fuelc (g)	Improvement
No.1	Rule	0.6	0.718	23	6360	-
	MPC		0.638	42	5926	6.8%
	t-MPC		0.613	37	5637	11.4%
No.2	Rule	0.65	0.718	22	6116	-
	MPC		0.628	48	5676	7.2%
	t-MPC		0.653	32	5594	8.5%
No.3	Rule	0.55	0.718	23	6597	-
	MPC		0.618	45	5986	9.3%
	t-MPC		0.596	40	5786	12.3%

B. ENERGY SAVING PERFORMANCE EVALUATION

In order to verify the superiority of the proposed method in energy-saving performance, rule-based method and traditional MPC method without considering the speed estimation uncertainty are used as benchmark.

1) RULE-BASED METHOD

When the SOC of the battery is initially at a high level (i.e. SOC>70%), the power demand of the vehicle can be fully covered by the battery, thus the vehicle works in pure electric mode. If the battery cannot meet the power demand, then the engine starts. If the difference between the required power of the vehicle and the power in the lowest fuel consumption range of the engine is less than 5%, the vehicle works in the engine drive mode. If the power demand is much higher, the vehicle works in the hybrid acceleration mode. At this time, the engine works in the high-efficiency zone as much as possible, and the insufficient power is supplemented by the power battery. When the battery SOC decreases to 50% after a period of power consumption, engine will be switched on to work near the upper boundary of the optimal area. The part exceeding the demand power is used for battery charging. When the SOC reaches 75%, it will switch to pure electric mode, engine drive mode or hybrid acceleration mode again.

2) TRADITIONAL MPC METHOD

This method is similar to the proposed method but without consideration of the speed error and tube effect, which means the uncertainty compensation part in speed predictor and the $w(h)$ in Eq.(15) is not considered. The state, action and cost function for this method is the same as that for the proposed method in this paper.

The speed trajectory used in Section V.A is also used here for energy-saving performance evaluation. Table.2 lists the comparison results, including the simulation of three groups

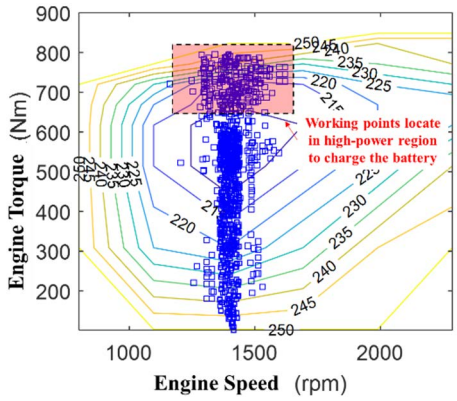

(a) Rule-based method

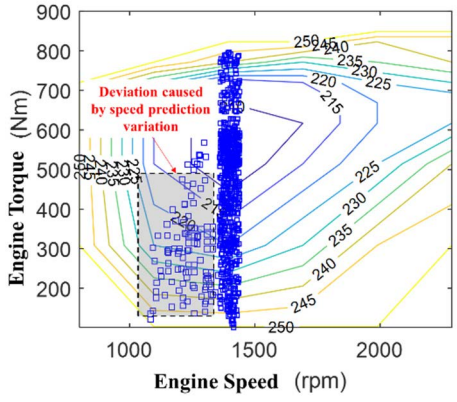

(b) Traditional MPC method

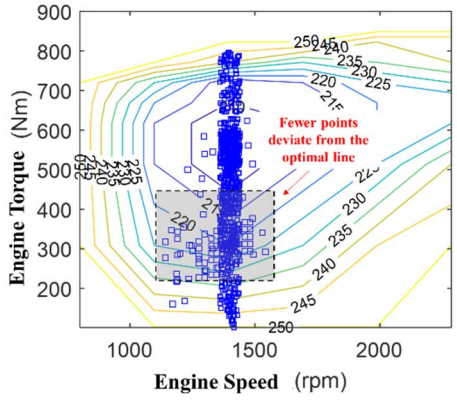

(c) Tube-MPC method

FIGURE 5. Working points distribution of the engine.

of different initial SOC. For fair comparison, the difference of SOC at the end has been weighted and incorporated into the final fuel consumption Fuel_c.

It can be seen from Table.2 that the proposed EMS considering speed prediction uncertainty has the lowest equivalent fuel consumption among the three methods. Compared with rule-based method, the proposed method can achieve 11.4%, 8.5% and 12.3% energy-saving improvement under the three defined initial SOC scenarios respectively. Compared with traditional MPC method, the proposed method is superior in terms of depressing the frequent start/stop of the engine and fuel consumption. By incorporating consideration of the speed prediction uncertainty into EMS, the stochastic variation in future power demand is fully evaluated by the tube mechanism in tube-MPC, thus make the control policy more careful about the future reward that could benefit from current action.

Fig.5 shows the working points distribution of the engine. It can be seen that for the rule-based method, there are many points locating in the high-power region with large fuel consumption rate. This is caused by the fact that when the SOC decreases to 50%, the engine will start to work with high power output not only satisfying the driving power demand but also charge the battery. This phenomenon greatly deteriorates the energy-saving performance under rule-based method. Traditional MPC method works much better than rule-based method, the points in high-power region is greatly depressed so the fuel consumption in this scenario is much lower. However, due to the uncertainty in speed prediction, the traditional MPC method cannot realize adaptive correction thus there are some points deviated from the optimal efficiency line. For the proposed tube-MPC method, the robustness and energy-saving performance are greatly enhanced by considering the uncertainty in speed prediction. Fewer points are deviated from the optimal working area.

VI. CONCLUSION

This paper proposes a predictive EMS framework considering uncertainty in speed estimation so that the energy-saving performance of EMS could be further enhanced. A speed predictor based on hybrid deep learning is proposed to extract temporal features that could reveal speed change mechanism. Then an online self-adaptive TPM is constructed to estimate the speed prediction uncertainty. Tube-MPC is used to solve the optimization control problem in a receding horizon manner. Simulations results show that the speed prediction accuracy is 47.4% and 23.1% higher than exponential decay rate prediction model and ARIMA model respectively. Compared with traditional rule-based and MPC method, the proposed tube-MPC method could achieve 10.7% and 3.0% energy-saving performance improvement in average.

Considering the fact that RL based EMS is attracting increasing attentions in recent years and has demonstrated desirable performance in efficiency improvement, future research may include a comprehensive comparison between RL based EMS and our proposed method to further improve the optimality of the uncertainty-aware predictive EMS framework. In addition, more uncertainty factors like HEV fuel consumption and battery SOC will be incorporated to verify the generalizability of our proposed method in the future.

APPENDIX

MATHEMATICAL MODEL OF HEV

The basic parameters of the investigated HEV is listed in Table.3. Fig.6 shows the topology of the power system of

the investigated HEV. The main components of the hybrid system include power battery, engine, integrated starter and generator (ISG) motor, drive motor and planetary gear. The planetary gear is a power coupling device, which coordinates the power among ISG motor, engine and drive motor. The carrier of the planetary gear is connected with the engine, the sun gear is connected with the ISG motor, and the ring gear is connected with the drive motor. In addition, the power battery is also connected with the drive motor and ISG motor to provide power source. In order to simplify the representation, the controller and other related parts are omitted. When the system works, the controller will optimize and adjust the power distribution between the power battery and the engine, and integrate the power into the driving motor through the planetary gears for power output to drive the vehicle forward. The mathematical models of the main components are as follows.

TABLE 3. Basic parameters of the investigated HEV.

parameter	value
Size	10460mm×24800mm×3310mm
Wheelbase	4800mm
Mass	12050kg
Highest speed	70km/h
Rolling resistance coefficient	0.016
Aerodynamic drag coefficient	0.68
Frontal area	5.05m2
Size	10460mm×24800mm×3310mm

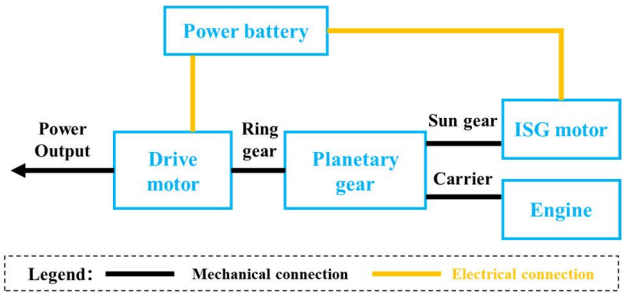

FIGURE 6. Topology of hybrid power system of the investigated HEV.

A. POWER BATTERY MODEL

Here, the first-order RC equivalent circuit model of the battery cell will be firstly established [43]. Then the model of battery pack will be derived according to the pack topology, which connects the characteristic parameters between the pack and the cell.

The first-order RC model mainly includes open circuit voltage (OCV), ohmic internal resistance R_s and RC network, which includes polarization resistance R_p and polarization capacitance C_p. According to Kirchhoff's law, the model satisfies the following state equation:

$$\begin{cases} \dot{V}_p = -\dfrac{V_p}{\tau} + \dfrac{i_b}{C_{batt}} \\ V_t = \mathrm{OCV} - V_p - i_b R_s \end{cases} \tag{17}$$

where V_p represents the terminal voltage of the RC network. τ is the time constant and theoretically $\tau = R_p C_p$. i_b represents excitation current. C_{batt} is the capacity of the power battery. V_t represents the terminal voltage. In the actual application, the above state equation needs to be discretized. According to the control theory, the discretized state equation is:

$$\begin{cases} V_p(k+1) = e^{-\frac{\Delta t}{\tau}} V_p(k) + i_b R_p (1 - e^{-\frac{\Delta t}{\tau}}) \\ V_p(0) = 0 \\ V_t(k) = \mathrm{OCV} - V_p(k) - i_b R_s \end{cases} \tag{18}$$

where k represents the time point index and ΔT represents the sampling period.

The battery pack is connected in series of 148 battery modules and each module is consisted of 3 cells in parallel. So the output voltage of the battery pack should be 148 times of the single cell. The ohmic resistance and polarization resistance of the pack should be multiplied by 148/3≈49.3 and the polarization capacitance of the pack should be divided by 49.3 on the basis of the cell calibration value.

B. ENGINE MODEL

Fig.7 shows the two main characteristics of the engine, including the external characteristic curve and fuel consumption curve. For the external curve, it reflects the mapping from engine speed n_{eng} to engine maximum torque $T_{eng-max}$ and can be expressed by:

$$T_{eng-max} = f_e(n_{eng}) \tag{19}$$

The maximum torque can only be achieved when the throttle opening achieves 100%. In this paper, we assume that the engine output torque T_{eng} is proportional to throttle opening γ and can be modeled by:

$$T_{eng} = \gamma T_{eng-max} \tag{20}$$

The instantaneous oil consumption $\dot{c}$ can be interpolated from the consumption map based on engine torque and engine speed, as shown in Fig.7(b). The mathematical model can be described by:

$$\dot{c} = \Gamma(n_{eng}, T_{eng}) \tag{21}$$

C. DRIVE MOTOR MODEL

The drive motor model includes external characteristic map and efficiency map. For the external characteristic map, under a certain speed n_{motor}, the torque of the motor T_{motor} shall be controlled within the maximum driving torque $T_{motor-max}$ and the maximum generation torque $T_{motor-min}$, which means:

$$\begin{aligned} f_{mg}(n_{motor}) &= T_{motor-min} \\ T_{motor-max} &= f_{md}(n_{motor}) \\ T_{motor-min} &\le T_{motor} \le T_{motor-max} \end{aligned} \tag{22}$$

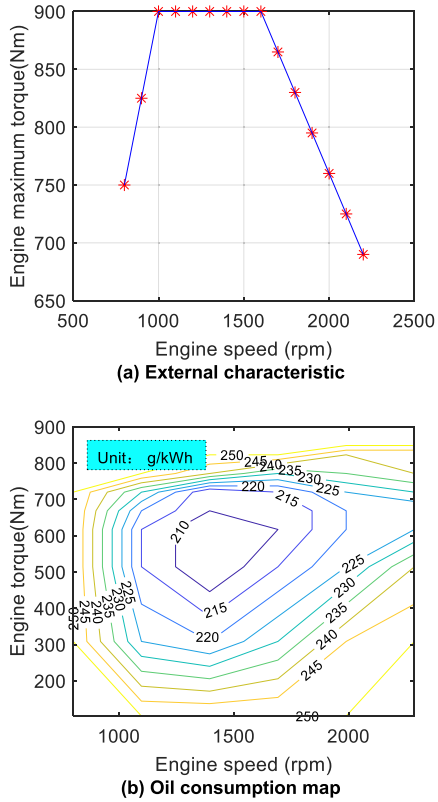

FIGURE 7. Characteristics of the engine.

For the efficiency map of the drive motor, like the oil consumption map of the engine, the efficiency of the motor η_{motor} is also the function of speed n_{motor} and torque T_{motor}, which can be expressed by:

$$\eta_{motor} = \Gamma(n_{motor}, T_{motor}) \tag{23}$$

D. IGS MODEL

The ISG motor also has the limitation of maximum torque, which can be described by following equation:

$$-T_{ISG-max} \leq T_{ISG} \leq T_{ISG-max} = f_{id}(n_{ISG}) \tag{24}$$

where T_{ISG} and n_{ISG} represent the output torque and speed of ISG motor, respectively.

In addition, because the ISG motor in this paper is mainly used to start the engine and adjust the speed of the engine in the acceleration mode, its working range is relatively narrow. According to the engineering experience, the efficiency of the ISG motor η_{ISG} is set to the fixed value of 90%.

E. ENERGY FLOW MODEL

The hybrid drive system studied in this paper has three working modes, namely pure electric mode, engine drive mode and hybrid mode. The hybrid mode can be further divided into acceleration mode and regenerative mode according to the discharging/charging state of power battery, as shown in Fig.8. In this subsection, the energy flow models under three modes are given.

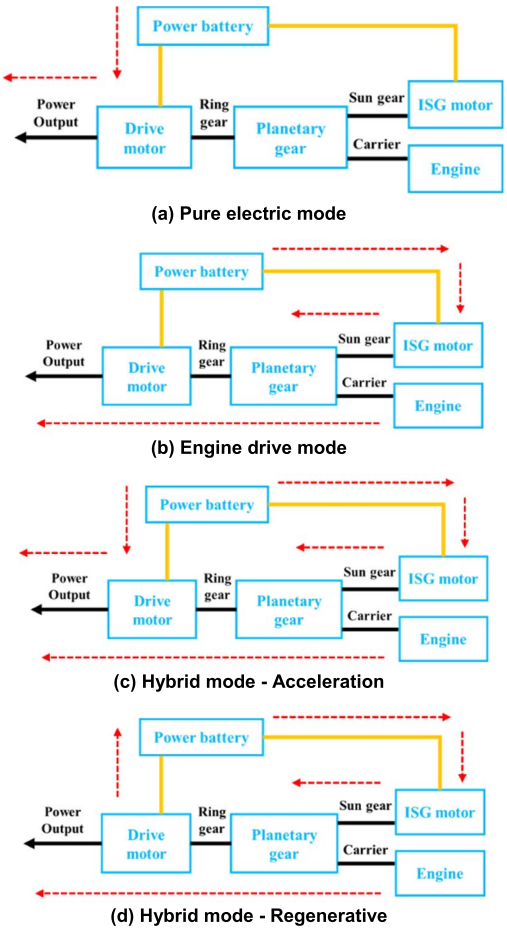

FIGURE 8. Different working modes of the investigated hybrid system.

As shown in Fig.8(a), in the pure electric mode, the vehicle uses the power battery as the sole power source to drive the vehicle. The ring gear connected to the drive motor will also rotate. The carrier connected to the engine will stay still while the ISG motor rotates in the opposite direction but without power consumption or power generation. The power of the motor satisfies the following equation:

$$P_{batt}\eta_{mech\_p} = P_{motor\_in} \tag{25}$$

where P_{batt} is the battery power and can be calculated by $P_{batt} = V_t i_b$. η_{mech_p} is the mechanical transmission efficiency of the planetary gear, which is taken as 94% here. P_{motor_in} indicates the input power of the motor.

In the process of power transmission from motor input to motor output, there is power loss due to motor efficiency, which meets the following equation:

$$P_{motor\_in}\eta_{motor} = P_{motor\_out} = T_{motor}n_{motor} \tag{26}$$

P_{motor_out} indicates the output power of the motor.

In addition, according to the mechanical connection topology, the drive motor is connected with the wheel through the main reducer, so the following speed conversion

equation is met:

$$u_a = 0.377\frac{rn_{motor}}{i_0} \tag{27}$$

where u_a is the vehicle speed. R is the radius of vehicle wheel. i_0 represents the transmission ratio of the main reducer, which is 6.14 here. The speed conversion equation determined by the mechanical connection topology is not only applicable to the pure electric mode, but also applicable to the engine drive mode and hybrid mode.

According to the power balance equation of the vehicle, the required power of the vehicle P_{veh} can be expressed as:

$$\begin{aligned} P_{veh} &= \left(mgf + \frac{C_D A u_a^2}{21.15} + mg\sin\alpha + m\frac{du_a}{dt}\right) u_a \\ &= P_{motor\_out}\eta_{mech} \end{aligned} \tag{28}$$

where m is the mass of the vehicle. g is the gravitational acceleration. f is rolling resistance coefficient. C_D is the aerodynamic drag coefficient. A is the frontal area. α represents the road incline, which is taken as 0 for simplicity here. η_{mech} refers to the mechanical efficiency from the output end of the motor to the wheel end after passing through the transmission parts such as the main reducer, which is taken as 96% according to engineering experience.

As shown in Fig.8(b), in the engine drive mode, the engine speed is coordinated by the ISG motor to drive the vehicle efficiently. According to the number of teeth of planetary gear and its connection relationship with various components, following kinetic equation can be obtained:

$$\begin{cases} n_{motor} = 1.36n_{eng} - 0.36n_{ISG} \\ T_{eng} = 0.73T_{motor} + 0.27T_{ISG} \end{cases} \tag{29}$$

In this mode, the following power balance relationship is satisfied:

$$T_{motor}n_{motor}\eta_{mech\_p} = P_{veh} \tag{30}$$

P_{veh} still meets the power balance relationship of Eq.(28). Considering that the power of ISG motor is provided by power battery, therefore:

$$T_{ISG}n_{ISG} = P_{batt} \tag{31}$$

As shown in Fig.8(c) and Fig.8(d), in the hybrid mode, the engine and drive motor work together to propel the vehicle, and the power balance meets the following relationship:

$$P_{batt} = P_{isg} + P_{motor\_in} \tag{32}$$

In addition, Eq.(26)∼Eq.(31) are still valid in this mode. In essence, the hybrid mode is the superposition of pure electric mode and engine drive mode. Therefore, integrating the speed transmission relationship and power balance relationship under pure electric mode and engine drive mode will result in the energy flow equation under hybrid mode.

The hybrid mode can be further divided into acceleration mode and regenerative mode, which mainly depends on the state of the battery. If the battery SOC is high, the engine and power battery jointly drive the vehicle forward, which is called acceleration mode. If SOC is low, in order to maintain the battery energy, the engine will output power higher than the driving demand and excess power will be used to charge the battery. This is called regenerative mode. Although there are some differences in energy flow direction between above two modes, there is no difference in dynamic equation due to the same mechanical connection topology. The difference between the two modes lies in the sign of P_{batt}, which is positive under acceleration mode and negative under regenerative mode.

F. OPTIMIZATION TARGET

HEV energy management should reduce fuel consumption as much as possible. In addition, to protect the power battery, the change of SOC should not be too drastic. Therefore, the cost function is defined as follows:

$$\min_{u'(h)} \sum_{t=h}^{h+n} \left[\chi\dot{c} + \varphi\left(\mathrm{SOC}\left(t\right) - \mathrm{SOC}_{sust}\right)^2 + \rho\right] T_s \tag{33}$$

where SOC_{sust} represents the balanced SOC value, which is set as 60% here. χ and φ are positive weight coefficients. T_S represents the sampling period. In addition, a penalty factor ρ is introduced into the cost function, which equals to 1 when engine starts or stops. This is to avoid frequent state switching of the engine. In particular, when the engine speed/torque or motor speed/torque exceeds the limit map during the state transition, an additional huge penalty (10^5 in this paper) will be introduced into the cost function to ensure that the engine and motor work within the allowable range.

REFERENCES

[1] Z. Qiao and C. Ding, "Recent progress on polyvinyl alcohol-based materials for energy conversion," *New J. Chem.*, vol. 46, no. 6, pp. 2586–2599, Feb. 2022.

[2] W. Zhou, N. Zhang, and H. Zhai, "Enhanced battery power constraint handling in MPC-based HEV energy management: A two-phase dual-model approach," *IEEE Trans. Transport. Electrific.*, vol. 7, no. 3, pp. 1236–1248, Sep. 2021.

[3] J. Moreno, M. E. Ortuzar, and J. W. Dixon, "Energy-management system for a hybrid electric vehicle, using ultracapacitors and neural networks," *IEEE Trans. Ind. Electron.*, vol. 53, no. 2, pp. 614–623, Apr. 2006.

[4] K. V. Singh, H. O. Bansal, and D. Singh, "Fuzzy logic and Elman neural network tuned energy management strategies for a power-split HEVs," *Energy*, vol. 225, Jun. 2021, Art. no. 120152.

[5] H. Jia, J. Tang, Y. Yu, Y. Sun, B. Yin, and C. Zhang, "Energy management strategy of fuel cell/battery hybrid vehicle based on series fuzzy control," *Int. J. Automot. Technol.*, vol. 22, no. 6, pp. 1545–1556, Dec. 2021.

[6] S. Mahapatra, T. Egel, R. Hassan, R. Shenoy, and M. Carone, "Model-based design for hybrid electric vehicle systems," *Sensors*, vol. 20, no. 5, p. 1362, 2020.

[7] C. Dextreit and I. V. Kolmanovsky, "Game theory controller for hybrid electric vehicles," *IEEE Trans. Control Syst. Technol.*, vol. 22, no. 2, pp. 652–663, Mar. 2014.

[8] L. Xianyang, "Simulation research on dynamic coordinated control of mode switching of parallel hybrid electric vehicle," M.S. dissertation, Beijing Jiaotong Univ., Beijing, China, 2014.

[9] T. Hofman, M. Steinbuch, R. M. van Druten, and A. F. A. Serrarens, "Rule-based energy management strategies for hybrid vehicle drivetrains: A fundamental approach in reducing computation time," *IFAC Proc. Volumes*, vol. 39, no. 16, pp. 740–745, 2006.

[10] B. V. Padmarajan, A. McGordon, and P. A. Jennings, "Blended rule-based energy management for PHEV: System structure and strategy," *IEEE Trans. Veh. Technol.*, vol. 65, no. 10, pp. 8757–8762, Oct. 2016.
[11] N. Jalil, N. A. Kheir, and M. Salman, "A rule-based energy management strategy for a series hybrid vehicle," in *Proc. Amer. Control Conf.*, Jun. 1997, pp. 689–693.
[12] J. Peng, H. He, and R. Xiong, "Rule based energy management strategy for a series–parallel plug-in hybrid electric bus optimized by dynamic programming," *Appl. Energy*, vol. 185, pp. 1633–1643, Jan. 2017.
[13] G. Pau, M. Collotta, and V. Maniscalco, "Bluetooth 5 energy management through a fuzzy-PSO solution for mobile devices of Internet of Things," *Energies*, vol. 10, no. 7, p. 992, Jul. 2017.
[14] D. Min, Z. Song, H. Chen, T. Wang, and T. Zhang, "Genetic algorithm optimized neural network based fuel cell hybrid electric vehicle energy management strategy under start-stop condition," *Appl. Energy*, vol. 306, Jan. 2022, Art. no. 118036.
[15] S. Hadj-Said, G. Colin, A. Ketfi-Cherif, and Y. Chamaillard, "Convex optimization for energy management of parallel hybrid electric vehicles," *IFAC-PapersOnLine*, vol. 49, no. 11, pp. 271–276, 2016.
[16] Z. Yuan, L. Teng, S. Fengchun, and H. Peng, "Comparative study of dynamic programming and Pontryagin's minimum principle on energy management for a parallel hybrid electric vehicle," *Energies*, vol. 6, no. 4, pp. 2305–2318, Apr. 2013, doi: 10.3390/en6042305.
[17] Y. Zhang, X. Jiao, L. Li, C. Yang, L. Zhang, and J. Song, "A hybrid dynamic programming-rule based algorithm for real-time energy optimization of plug-in hybrid electric bus," *Sci. China Technol. Sci.*, vol. 57, no. 12, pp. 2542–2550, Dec. 2014.
[18] F. C. Correa, J. J. Eckert, L. C. A. Silva, M. Martins, V. Baroncini, F. M. Santiciolli, C. Goncalves, and F. G. Dedini, "Rule-based control and fuzzy control for power management strategies for hybrid vehicles," in *Proc. IEEE Colombian Conf. Appl. Comput. Intell. (IEEE ColCACI)*, Aug. 2020, pp. 1–6.
[19] J. Liu, Y. Chen, W. Li, F. Shang, and J. Zhan, "Hybrid-trip-model-based energy management of a PHEV with computation-optimized dynamic programming," *IEEE Trans. Veh. Technol.*, vol. 67, no. 1, pp. 338–353, Jan. 2018.
[20] N. Guo, X. Zhang, Y. Zou, G. Du, C. Wang, and L. Guo, "Predictive energy management of plug-in hybrid electric vehicles by real-time optimization and data-driven calibration," *IEEE Trans. Veh. Technol.*, early access, Dec. 21, 2021, doi: 10.1109/TVT.2021.3138440.
[21] N. Guo, X. Zhang, Y. Zou, L. Guo, and G. Du, "Real-time predictive energy management of plug-in hybrid electric vehicles for coordination of fuel economy and battery degradation," *Energy*, vol. 214, Jan. 2021, Art. no. 119070, doi: 10.1016/j.energy.2020.119070.
[22] X. Tang, T. Jia, X. Hu, Y. Huang, Z. Deng, and H. Pu, "Naturalistic data-driven predictive energy management for plug-in hybrid electric vehicles," *IEEE Trans. Transport. Electrific.*, vol. 7, no. 2, pp. 497–508, Sep. 2020.
[23] N. Guo, B. Lenzo, X. Zhang, Y. Zou, R. Zhai, and T. Zhang, "A real-time nonlinear model predictive controller for yaw motion optimization of distributed drive electric vehicles," *IEEE Trans. Veh. Technol.*, vol. 69, no. 5, pp. 4935–4946, May 2020, doi: 10.1109/TVT.2020.2980169.
[24] J. Xu, Z. Li, L. Gao, J. Ma, Q. Liu, and Y. Zhao, "A comparative study of deep reinforcement learning-based transferable energy management strategies for hybrid electric vehicles," 2022, *arXiv:2202.11514*.
[25] T. Liu, X. Hu, S. E. Li, and D. Cao, "Reinforcement learning optimized look-ahead energy management of a parallel hybrid electric vehicle," *IEEE/ASME Trans. Mechatronics*, vol. 22, no. 4, pp. 1497–1507, Aug. 2017.
[26] M. Li, M. Yan, H. He, and J. Peng, "Data-driven predictive energy management and emission optimization for hybrid electric buses considering speed and passengers prediction," *J. Cleaner Prod.*, vol. 304, Jul. 2021, Art. no. 127139.
[27] X. Guo, X. Yan, Z. Chen, and Z. Meng, "A novel closed-loop system for vehicle speed prediction based on APSO LSSVM and BP NN," *Energies*, vol. 15, no. 1, p. 21, Dec. 2021.
[28] M. R. Amini, Y. Feng, Z. Yang, I. Kolmanovsky, and J. Sun, "Long-term vehicle speed prediction via historical traffic data analysis for improved energy efficiency of connected electric vehicles," *Transp. Res. Rec. J. Transp. Res. Board*, vol. 2674, no. 11, pp. 17–29, Nov. 2020.
[29] B. Suh, Y. Shao, and Z. Sun, "Vehicle speed prediction for connected and autonomous vehicles using communication and perception," in *Proc. Amer. Control Conf. (ACC)*, Jul. 2020, pp. 448–453.
[30] J. Shangguan, H. Guo, and M. Yue, "Robust energy management of plug-in hybrid electric bus considering the uncertainties of driving cycles and vehicle mass," *Energy*, vol. 203, Jul. 2020, Art. no. 117836.
[31] J. He, C. Shi, T. Wei, X. Peng, and Y. Guan, "Hierarchical optimal energy management strategy of hybrid energy storage considering uncertainty for a 100% clean energy town," *J. Energy Storage*, vol. 41, Sep. 2021, Art. no. 102917.
[32] S. Xie, X. Hu, Z. Xin, and L. Li, "Time-efficient stochastic model predictive energy management for a plug-in hybrid electric bus with an adaptive reference state-of-charge advisory," *IEEE Trans. Veh. Technol.*, vol. 67, no. 7, pp. 5671–5682, Jul. 2018.
[33] Y. Li, "An energy management method of electric vehicles based on stochastic model predictive control," in *Proc. IEEE 4th Adv. Inf. Manage., Communicates, Electron. Automat. Control Conf. (IMCEC)*, Jun. 2021, pp. 1757–1761.
[34] X. Zeng and J. Wang, "A parallel hybrid electric vehicle energy management strategy using stochastic model predictive control with road grade preview," *IEEE Trans. Control Syst. Technol.*, vol. 23, no. 6, pp. 2416–2423, Nov. 2015.
[35] M. Zhao, R. Zhang, C. Lin, H. Zhou, and J. Shi, "Stochastic model predictive control for dual-motor battery electric bus based on signed Markov chain Monte Carlo method," *IEEE Access*, vol. 8, pp. 120785–120797, 2020.
[36] J. Hanema, M. Lazar, and R. Tóth, "Heterogeneously parameterized tube model predictive control for LPV systems," *Automatica*, vol. 111, Jan. 2020, Art. no. 108622.
[37] J. Li, C. Wu, R. Song, Y. Li, W. Xie, L. He, and X. Gao, "Deep hybrid 2-D-3-D CNN based on dual second-order attention with camera spectral sensitivity prior for spectral super-resolution," *IEEE Trans. Neural Netw. Learn. Syst.*, early access, Aug. 4, 2021, doi: 10.1109/TNNLS.2021.3098767.
[38] A. Gallardo-Antolín and J. M. Montero, "Detecting deception from gaze and speech using a multimodal attention LSTM-based framework," *Appl. Sci.*, vol. 11, no. 14, p. 6393, Jul. 2021.
[39] L. Teng, H. Gao, L. Li, and D. Cao, "Adaptive energy management for real driving conditions via driving cycle transformation and reinforcement learning," 2018, *arXiv:2007.12560*.
[40] J. Peng, L. Zhang, Q. Chen, R. Long, K. Zhou, Z. Liu, and H. Su, "Anti-disturbance TUBE MPC method of wireless power transmission system based on state feedback," *Energy Rep.*, vol. 7, pp. 411–418, Apr. 2021.
[41] G. Bastos and E. Franco, "Energy shaping dynamic tube-MPC for underactuated mechanical systems," *Nonlinear Dyn.*, vol. 106, no. 1, pp. 359–380, Sep. 2021.
[42] X. Zhang, Y. Zou, J. Fan, and H. Guo, "Usage pattern analysis of Beijing private electric vehicles based on real-world data," *Energy*, vol. 167, pp. 1074–1085, Jan. 2019.
[43] T. Zhang, N. Guo, X. Sun, J. Fan, N. Yang, J. Song, and Y. Zou, "A systematic framework for state of charge, state of health and state of power co-estimation of lithium-ion battery in electric vehicles," *Sustainability*, vol. 13, no. 9, p. 5166, May 2021.